In vivo implantation of 3-dimensional printed customized branched tissue engineered vascular graft in a porcine model

Enoch Yeung, MBBS,[a] Takahiro Inoue, MD, PhD,[a] Hiroshi Matsushita, MD,[a] Justin Opfermann, MS,[b] Paige Mass, BS,[b] Seda Aslan, MS,[c] Jed Johnson, PhD,[d] Kevin Nelson, PhD,[d] Byeol Kim, BS,[c] Laura Olivieri, MD,[b] Axel Krieger, PhD,[c] and Narutoshi Hibino, MD, PhD[a,e]

ABSTRACT

Background: The customized vascular graft offers the potential to simplify the surgical procedure, optimize physiological function, and reduce morbidity and mortality. This experiment evaluated the feasibility of a flow dynamic–optimized branched tissue engineered vascular graft (TEVG) customized based on medical imaging and manufactured by 3-dimensional (3D) printing for a porcine model.

Methods: We acquired magnetic resonance angiography and 4-dimensional flow data for the native anatomy of the pigs (n = 2) to design a custom-made branched vascular graft of the pulmonary bifurcation. An optimal shape of the branched vascular graft was designed using a computer-aided design system informed by computational flow dynamics analysis. We manufactured and implanted the graft for pulmonary artery (PA) reconstruction in the porcine model. The graft was explanted at 4 weeks after implantation for further evaluation.

Results: The custom-made branched PA graft had a wall shear stress and pressure drop (PD) from the main PA to the branch PA comparable to the native vessel. At the end point, magnetic resonance imaging revealed comparable left/right pulmonary blood flow balance. PD from main PA to branch between before and after the graft implantation was unchanged. Immunohistochemistry showed evidence of endothelization and smooth muscle layer formation without calcification of the graft.

Conclusions: Our animal model demonstrates the feasibility of designing and implanting image-guided, 3D-printed, customized grafts. These grafts can be designed to optimize both anatomic fit and hemodynamic properties. This study demonstrates the tremendous potential structural and physiological advantages of customized TEVGs in cardiac surgery. (J Thorac Cardiovasc Surg 2020;159:1971-81)

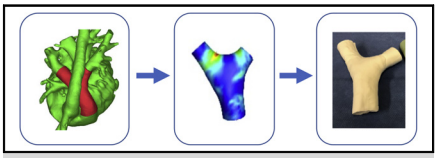

In vivo evaluation of our flow-optimized customized vascular graft via virtual planning.

CENTRAL MESSAGE

Our integrated virtual surgical planning and flow dynamic profile optimization prove the feasibility of providing an optimized anatomy and hemodynamic parameter of the 3D printed, customized vascular graft.

PERSPECTIVE

Each patient with congenital heart disease has a unique vascular defect and hemodynamic profile. Therefore, there is a need for a "best fit" conduit to provide the optimal long-term outcome. This study demonstrates that our integrated approach combining virtual surgical planning, 3-dimensional printing, and electrospinning to create a customized vascular graft can provide an optimized anatomic and hemodynamic result in vivo.

See Commentaries on pages 1982 and 1984.

One of the leading causes of death in newborns is congenital cardiac anomalies.[1] Owing to the anatomic complexity and uniqueness of each vascular defect and the individual physiology of the circulatory system, congenital vascular reconstructive surgery can be very challenging. There is an unmet clinical need for individually customized grafts

From the [a]Division of Cardiac Surgery, Johns Hopkins Hospital, Baltimore, Md; [b]Division of Cardiology, Children's National Medical Center, Washington, DC; [c]Department of Mechanical Engineering, University of Maryland, Baltimore, Md; [d]Nanofiber Solutions, Hilliard, Ohio; [e]Department of Cardiac Surgery, University of Chicago/Advocate Children's Hospital, Chicago, Ill.

Drs Olivieri, Krieger, and Hibino are co–principal investigators of this study.

This work was funded by National Institutes of Health Grants R21/33 R21HD090671, 4R33HD090671-03.

Read at the 99th Annual Meeting of The American Association for Thoracic Surgery, Toronto, Ontario, Canada, May 4-7, 2019.

Received for publication May 15, 2019; revisions received Sept 15, 2019; accepted for publication Sept 16, 2019; available ahead of print Dec 19, 2019.

Address for reprints: Narutoshi Hibino, MD, PhD, Department of Cardiac Surgery, The University of Chicago, 5841 S Maryland Ave, Chicago, IL 60637 (E-mail: nhibino@surgery.bsd.uchicago.edu).

0022-5223/$36.00

https://doi.org/10.1016/j.jtcvs.2019.09.138

CONG

Abbreviations and Acronyms

3D = 3-dimensional
CAD = computer-aided design
CFD = computational fluid dynamics
CPB = cardiopulmonary bypass
IVC = inferior vena cava
LPA = left pulmonary artery
MPA = main pulmonary artery
MRA = magnetic resonance angiography
MRI = magnetic resonance imaging
PA = pulmonary artery
PCL = polycaprolactone
PD = pressure drop
PLCL = poly-L-lactide-co-ε-caprolactone
RPA = right pulmonary artery
SMA = α-smooth muscle actin
SMC = smooth muscle cell
STL = stereolithography
TEVG = tissue engineered vascular graft

Scanning this QR code will take you to the article title page to access supplementary information. To view the AATS Annual Meeting Webcast, see the URL next to the webcast thumbnail.

in congenital vascular repair. Pediatric vascular reconstruction carries an increased risk of graft complications, such as rapid graft dysfunction, anastomotic stricture formation, size mismatch–related geometric disruption, and pulmonary artery (PA) obstruction owing to the patients' rapid growth rate.[2-5] Mismatched vasculature calibers, lack of growth potential, suboptimal biocompatibility, and risk of thromboembolic events make the use of synthetic implants for congenital vascular reconstructive an unsettling choice.[6-8]

In the last decade, 3D printing has been used in the manufacture of tissue engineered vascular grafts (TEVGs). This technology offers the potential to develop a customized biodegradable scaffold to promote cellular proliferation and maturation, leading to the formation of a physiologically functional blood vessel. For congenital vascular repair, the customized TEVG provides an opportunity for high-fidelity anatomic reconstruction of vasculature with growth potential. This can significantly improve the clinical outcomes. Our previous study in an ovine model validated the concept of 3D-printed customized TEVGs using a simple straight vascular graft. Our results showed that the

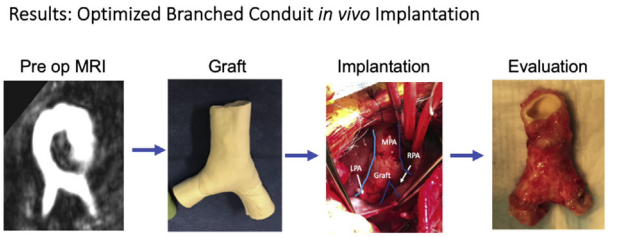

VIDEO 1. Objectives and methodology of optimization and in vivo implantation of the customized branched tissue engineered vascular graft. Video available at: https://www.jtcvs.org/article/S0022-5223(19)32170-1/fulltext.

TEVGs were biocompatible with adequate neotissue formation and had mechanical properties comparable to those of the native tissue with a 6-month follow-up after inferior vena cava (IVC) transposition surgery.[9]

The unique aspects to consider for cardiovascular surgery include a dynamic fluid profile of the circulatory system and the physiological compliance of the vasculature. Thus, the long-term surgical outcomes of the grafts are based not only on anatomic specificity, but also on the growth potential of the TEVG to match the size of the growing patient. The TEVG must maintain the fluid dynamic profile of the circulation system to achieve a successful long-term clinical outcome. Our group previously introduced a novel preoperative virtual surgical planning strategy in silico for the Fontan procedure.[10] This study established that preoperative virtual surgical planning can be used to optimize a conduit design that improves the hemodynamic profile after surgery.

Although a feasibility analysis was performed for a simple straight TEVG in our previous study, a curvilinear or branched TEVG is needed to address cases involving complex anatomy for clinical use. Thus, in this study, we built on previous work by creating a branched and curved TEVG to evaluate the potential to design and implant complex- shaped TEVGs in vivo (Video 1). As a preclinical experiment, the goal of this study was to investigate the feasibility to fabricate patient-specific TEVGs with computational fluid dynamics (CFD) optimization for reconstruction of the central PA (Figure 1). Central PA reconstructive surgery plays an important role in many surgical procedures performed to repair congenital cardiac defects in neonates and young infants.[11] We then evaluated the short-term outcomes of the conduit optimized by CFD hemodynamic analysis in a porcine model for a 1-month trial period. (Figure 2)

MATERIALS AND METHODS

Preoperative Imaging, 3D Model Design, and Scaffold Fabrication

Cardiac magnetic resonance imaging (MRI) was performed 4 to 5 weeks before implantation, along with magnetic resonance angiography (MRA)

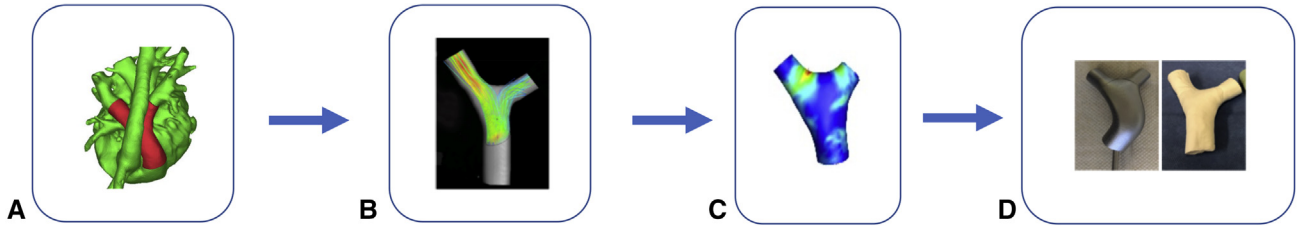

FIGURE 1. Flow chart descripting the manufacturing process of image guided customized tissue-engineered graft. A, Creation of the 3-dimensional (3D) vascular image of the native model from the magnetic resonance imaging segmentation technique, in which the 3D image of the vasculature is created from the summation of individual 2-dimensional image. B, Optimization of the conduit design with the iteron using iterative strategy. C, Computational fluid dynamics optimization of the 3D printed customized graft. D, Manufacture of the nanofiber graft via electrospinning technology. (*Left*) Stainless-steel mandrel; (*right*) graft.

and phase-contrast flow analysis using both 2D and 4D flow acquisitions. Following MRI, MRA was used as a roadmap to build a 3D digital model of the central PA reconstruction, using commercially available image segmentation software (Mimics; Materialise, Leuven, Belgium). Both automatic thresholding and manual methods were used to identify the blood pool of the right ventricular outflow tract and branch PAs in each MRA slice. Based on species-specific growth curves, a small increase in dimension (both length of the outflow tract and diameter of the PAs) was added to the blood pool segmentation to account for growth of the animal during the 30 days between imaging and surgery. This segmentation was converted into a 3D digital model, which was then exported using the stereolithography (STL) file format. This STL file was converted into a computer-aided design (CAD) file, smoothed, and hollowed using computer-aided design software (3-matic; Materialise and SolidWorks; Dassault Systemes, Waltham, Mass).

After validation of the design, a biodegradable version of each conduit was manufactured using a 3D electrospinning technique. For the electrospinning, a stainless-steel mandrel in the shape of the optimized graft was 3D-printed by exporting the STL file of the graft to an external printing house (Protolabs, Rosemount, Minn). The mandrel was designed such that the electrospun polymer graft could be removed. The mandrel was a 5-part piece consisting of the main PA (MPA), distal right PA (RPA), proximal RPA, distal left PA (LPA), and proximal LPA pinned together that could be taken apart for the graft removal step. An additional pin is added to the mandrel to clamp it into the electrospinning setup.

The biodegradable nanofiber material composed of a 1:1 ratio of polycaprolactone (PCL) and poly-L-lactide-co-ε-caprolactone (PLCL) were electrospun to coat the 3D-printed mandrel (Nanofiber Solutions, Hilliard, Ohio) (Figure E1). By applying high voltage to the polymer solution, polymer fibers are deposited on the mandrel to create the graft. After deposition of the fibers, the mandrel was disassembled, and the electrospun graft was removed. The graft was placed in a standard Tyvek pouch and subjected to low-temperature sterilization with vaporized hydrogen peroxide and ozone (STERIZONE VP4; Getinge, Getinge, Sweden).

Graft Implantation in Vivo

The Animal Care and Use Committee at Johns Hopkins Hospital approved the care, use, and monitoring of animals for these experiments. The animals received humane care in compliance with the National Institutes of Health's Guide for the Care and Use of Laboratory Animals. The graft was implanted as central PA reconstruction in the porcine model (mean body weight, 35 kg). The animal size increased by roughly one-third over the 1-month study period (mean body weight, 45 kg). The pigs were anesthetized with 1.5% isoflurane during surgery. The surgery was performed at the left thoracotomy position, the LPA and RPA were exposed and isolated, and heparin (100 IU/kg) was administered intravenously. During the procedure, cardiopulmonary bypass (CPB) was performed. The graft was implanted to replace main and branch PAs as an interposition graft using 6-0 Prolene suture. Antibiotic treatment (cefazolin 22 mg/kg intravenously) was administered intraoperatively and at 7 days

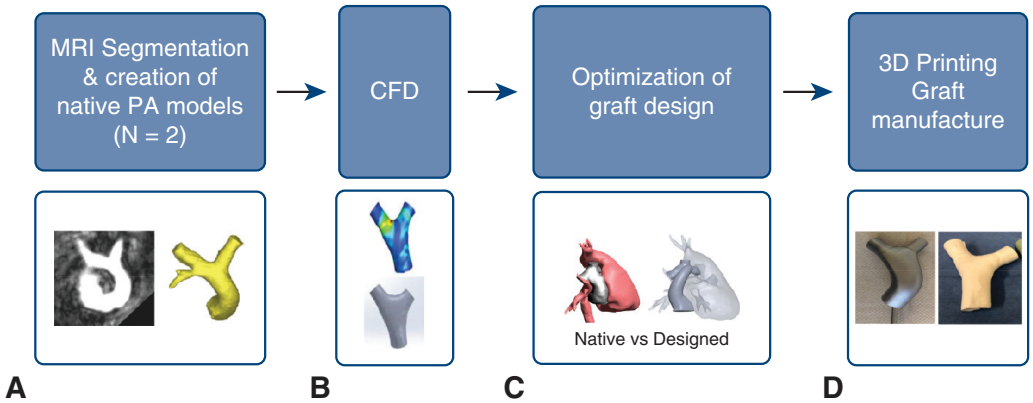

FIGURE 2. A, Graft manufacture begins with magnetic resonance imaging (*MRI*) acquisition with the MRI segmentation technology. B, It follows by computational flow dynamics (*CFD*) analysis of the flow dynamics of the images of vasculatures created. C, Optimization of the flow dynamics of the graft occurs after CFD analysis. D, After optimization, the graft is fabricated by 3D electrospinning technology. (*Right*) Mandrel for electrospinning; (*left*) graft. *PA*, Pulmonary artery.

postoperatively. All pigs were maintained on a daily oral dose of aspirin (81 mg/day) until the 1-month endpoint. The animals were imaged with an identical cardiac MRI protocol at 1 month postoperatively, prior to sacrifice.

Histology and Immunohistochemistry

Explanted TEVG samples were fixed in 10% formalin for 24 hours at 4°C and then embedded in paraffin. Standard histology was done using staining of tissue sections with hematoxylin and eosin, Masson trichrome, Verhoeff-Van Gieson, and von Kossa stains. Immunohistochemistry was performed using the following primary antibodies: von Willebrand factor (1:2000; Dako, catalog A0082), α-smooth muscle actin (SMA) (1:500; Abcam, catalog ab5694), and CD68 (1:200; Abcam, ab31630). Detection of antibody binding was done using biotinylated secondary antibodies (Vector Laboratories, Burlingame, Calif), followed by incubation with streptavidinated horseradish peroxidase (Vector Laboratories). A chromogenic reaction with 3,3-diaminobenzidine (Vector Laboratories) was performed for the development of immunohistochemistry. Counterstaining of the nuclei was done with Gill's hematoxylin (Vector Laboratories).

Histological and Quantitative Analyses

The remaining scaffold area was measured by hematoxylin and eosin staining and plain (polarized light) histology. The thickness of the smooth muscle layer from the graft was measured by SMA staining using ImageJ software (National Institutes of Health, Bethesda, Md). The thickness of the muscle layer was quantified by analyzing the muscular thickness–to–full-thickness ratio of the graft to that of the native tissue from a representative section of each sample and averaging the value for all samples (n = 5). The remaining scaffold area was quantified by analyzing the light intensity under polarized light microscopy the same exposure time and the pixel calculation from a representative section of each sample and averaging the value for all samples (n = 5).

Biochemical Analysis

The Sircol colorimetric assay (Biocolor, Carrickfergus, United Kingdom) was used to evaluate the collagen content. In accordance with the assay's protocol, we measured 100 mg dry weight of each sample and transferred it to low-protein-binding 1.5-mL conical microcentrifuge tubes with 1.0 mL of pepsin (Sigma-Aldrich, St Louis, Mo), with a concentration of 0.1 mg/mL of 0.5 M acetic acid to solubilize the collagen by overnight incubation. The collagen content in each sample was evaluated by assessing the absorbance intensity at 555 nm after dye binding according to the manufacturer's protocol.

Statistical Analysis

In this experiment, data from CFD simulation and histological analysis are represented graphically as bar or line charts with error bars representing the mean with standard error of the mean. The unpaired 2-tailed *t* test was used for the analysis of collagen. The Pearson correlation coefficient was used to determine the significance of any correlation of SMA/high-power field. A P value <.05 was considered statistically significant. Statistical analysis was performed using Prism version 8 (GraphPad Software, La Jolla, Calif).

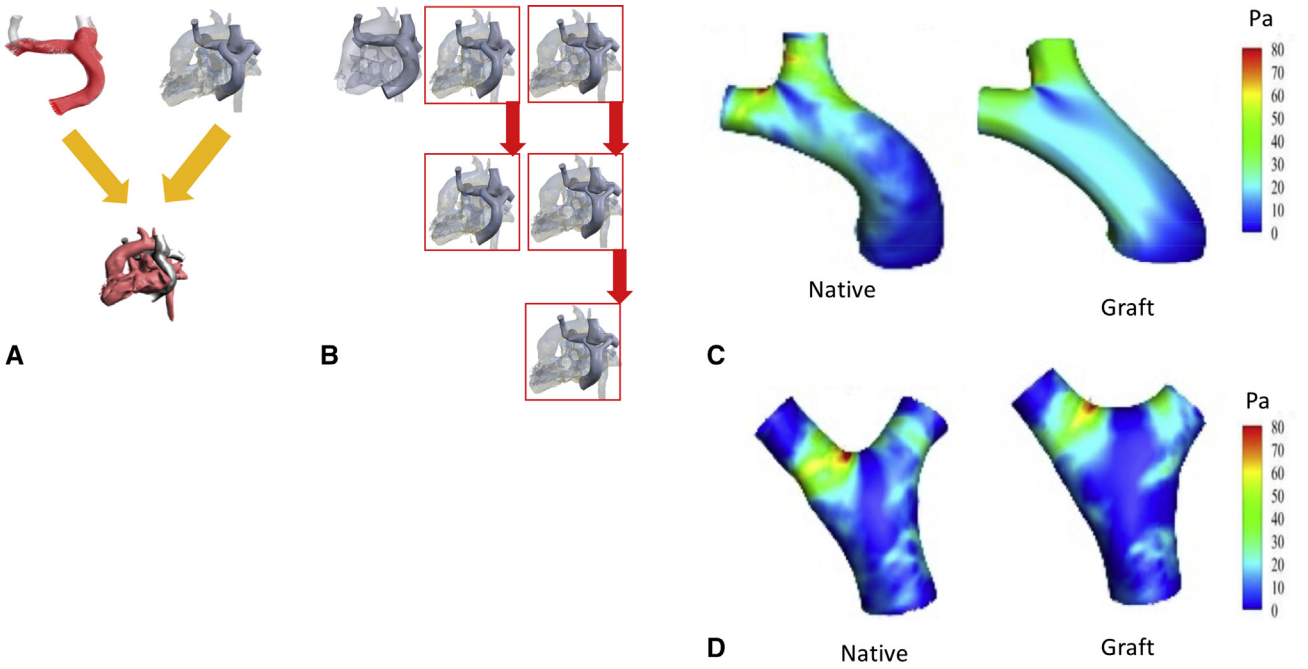

FIGURE 3. A and B, Diagram illustrating the iteration optimization strategy via surgical virtual planning. A, The 3D model of the surrounding heart and vasculature anatomy overlaid with the new graft designs, to minimize any overlap between the optimized graft and other thoracic structures. B, The design with the best performance was determined for the next iteration of simulation using computational fluid dynamics. C and D, The wall shear stress distribution of the porcine models is represented in different colors, with *blue* indicating the minimum and *red* the maximum as the reference in the left sidebar. The power loss between the inlet and the outlet of the graft compared to the native model is shown, along with the wall shear stress distribution in the native tissue and the graft. C, Porcine model 1. Power loss: native vs designed, 1.5×10^{-2} W vs 1.4×10^{-2} W; wall shear stress distribution: native vs designed, 2 Pa vs 2.16 Pa. D, Porcine model 2. Power loss: native vs designed, 2.35×10^{-3} W vs 1.65×10^{-3} W; wall shear stress distribution: native vs designed, 1.14 Pa vs 1.02 Pa. Overall, the wall shear stress distribution in the 2 porcine models was similar in the native tissue and graft.

RESULTS

Optimization of the Custom-Made Graft With CFD Simulation

Optimization of the graft was done using an iterative strategy as described previously.[10] First, with all the designed CAD models, the model of the surrounding heart and vasculature anatomy was overlaid with the new graft designs, to minimize any overlap between the optimized graft and other thoracic structures (Figure 3, *A*). Grafts with different feasible anatomic designs were chosen. The CFD simulation optimized the graft based on 3 parameters: (1) reduction of power loss across the conduit inlet and outlet, (2) adjustment of the even fluid flow between the right and left branches, and (3) wall shear stress distribution optimization. The design with the best performance was determined for the next iteration of the simulation (Figure 3, *B*).

The CFD analysis was performed with the hemodynamic parameters considered in this study, including power loss, flow distribution (LPA:RPA), and wall shear stress. The power loss was calculated based on the changes in pressure and flow rates on inlets and outlet of each model as described previously.[10] The wall shear stress distribution of the porcine model is shown in Figure 3, *C* and *D*. In the porcine models 1 and 2, compared with the preoperative native model, the simulation model has a similar power loss between the inlet and the outlet of the graft (pig 1: native vs designed, 1.5×10^{-2} W vs 1.4×10^{-2} W; pig 2: native vs designed, 2.35×10^{-3} W vs 1.65×10^{-2} W). The flow distribution was maintained with a similar flow in the both the native and designed conduits (pig 1: LPA:RPA, 47:53; pig 2: LPA:RPA, 42:58). The wall shear stress was comparable in the native tissue and graft (pig 1: native vs designed, 2 Pa vs 2.16 Pa; pig 2: native vs designed, 1.14 Pa vs 1.02 Pa) (Figure 3, *C* and *D*). Overall, the designed models demonstrated comparable hemodynamic and wall shear stress to the native models.

In Vivo Implantation of the Customized Conduit

The preoperative vasculature images were prepared with MRI for CAD image creation (Figure 4, *A*). Preoperative LPA:RPA blood flow balance was recorded (LPA:RPA, 45:55) (Figure 4, *F*). The customized branched TEVG was fabricated via 3D electrospinning technology (Figure 4, *B*). Graft implantation surgery was performed as described above (Figure 4, *C*). At 1 month after graft implantation, postoperative MRI was performed (Figure 4, *D*), and LPA:RPA blood flow balance in the optimized graft design was measured (LPA:RPA, 52:48) (Figure 4, *G*). At the end of the study, the graft was explanted for macroscopic

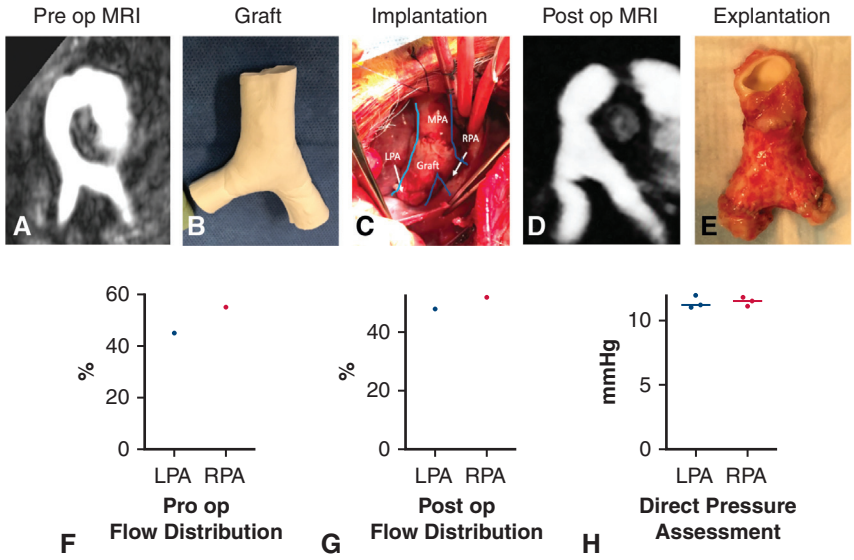

FIGURE 4. Study design of the in vivo implantation of computational fluid dynamics–optimized tissue engineered vascular graft (TEVG). A, Preoperative magnetic resonance imaging (*MRI*) of the porcine model vasculature. B, 3D-printed branched TEVG with the optimized design. C, Intraoperative picture of the implanted conduit. The *blue lines* outline the implanted graft intraoperatively. D, Postoperative MRI of the porcine model vasculature. E, The explanted graft at the end point of the experiment. F and G, Flow distribution measurement via MRI across the left pulmonary artery (*LPA*) and right pulmonary artery (*RPA*) preoperatively and postoperatively F, Flow distribution measurement by MRI across the LPA and RPA preoperatively. G, Postoperative imaging analysis demonstrating comparable left/right pulmonary blood flow balance with improvement of the flow balance in the optimized graft design (LPA:RPA, preoperative, 45:55; postoperative, 48:52). H, Intraoperative direct RPA and LPA blood pressure was measured; both were of the same magnitude (mean LPA:RPA blood pressure, 11.93:11.80 mm Hg). The *middle horizontal line* represents the median; the upper and lower *whiskers* represent the maximum and minimum values of nonoutliers.

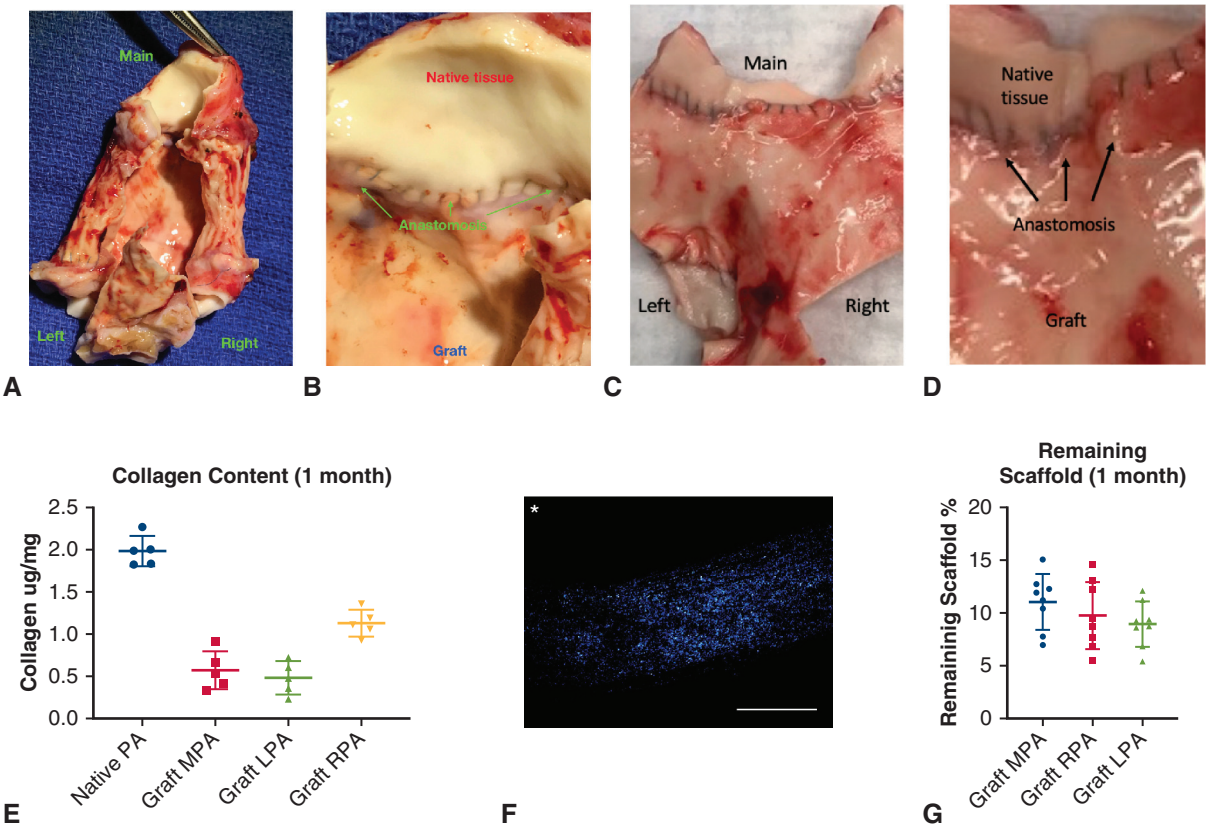

FIGURE 5. A-D, Graft evaluation after explantation at 1 month after surgery. There was no clot formation macroscopically. A and B, Pig 1. A, The explanted graft as a whole. B, The anastomosis interface of the graft. C and D, Pig 2. C, The explanted graft as a whole. D, The anastomosis interface of the graft. E, The collagen content determined by Sircol colorimetric assay (native vs MPA vs LPA vs RPA: 1.89 ± 0.18 vs 0.57 ± 0.23 vs 0.48 ± 0.19 vs 1.13 ± 0.16 μg/mg). F, Representative of the visualization of the remaining scaffold from the polarized light microscopy. The *blue color* indicates the remaining scaffold. *Lumen side. (Scale bar: 1000 μm.) G, The remaining scaffold percentages in individual parts of the graft. The average of remaining scaffold in the main PA, right PA, and left PA in porcine model were 11.0 ± 2.64, 9.76 ± 3.18, and 8.93 ± 2.14, respectively. (Scale bar: 1000 μm.) *PA*, Pulmonary artery; *MPA*, main pulmonary artery; *LPA*, left pulmonary artery; *RPA*, right pulmonary artery.

inspection (Figure 4, *E*), and direct blood pressure measurements in the LPA and RPA were obtained (Figure 4, *H*). The magnitudes of LPA and RPA pressure were roughly 11 to 12 mm Hg. The absence of clinically significant stenosis was demonstrated by an almost equal flow distribution and similar pressure within the PA branches.

Biocompatibility of the Graft

The biocompatibility of the graft, including patency and tissue degradation, was evaluated after 1-month. No graft-related stenosis, dilation, or rupture occurred by the 1-month endpoint of the study, and there was no clot formation macroscopically or microscopically (Figure 5, *A-D*). The presence of collagen in the graft was verified by collagen assay, suggesting ongoing collagen tissue formation (Figure 5, *E*). The graft degradation was detected by the presence of remaining scaffold area from the polarized light microscopy (Figure 5, *F*). The remaining scaffold area in the individual parts of the graft was measured; the averages of the remaining scaffold area in the models were 11.01 ± 2.64% for of MPA, 9.76 ± 3.18% for RPA, and 8.93 ± 2.14% for LPA (Figure 5, *G*).

Formation of Neotissue and Vasculature

Extracellular matrix formation was evaluated with Mason Trichrome staining. Compared with the native tissue (Figure 6, *A*, *F*, and *K*), the vascular graft showed ongoing extracellular matrix formation. (Figure 6, *B*, *G*, and *L*). Von Kossa staining demonstrated no ectopic calcification (Figure 6, *C*, *H*, and *M*). SMC layers contribute to vascular function and were evaluated by SMA immunohistochemistry staining. The presence of multilayered SMA-positive cells in the graft compared with the native pulmonary tissue suggests ongoing active vascular muscle remodeling (Figure 6, *D*, *I*, and *N*).

Endothelial cell formation in the graft was shown with the von Willebrand factor–positive cells in the graft (Figure 6, *E*, *J*, and *O*). The presence of $CD68^{+}$

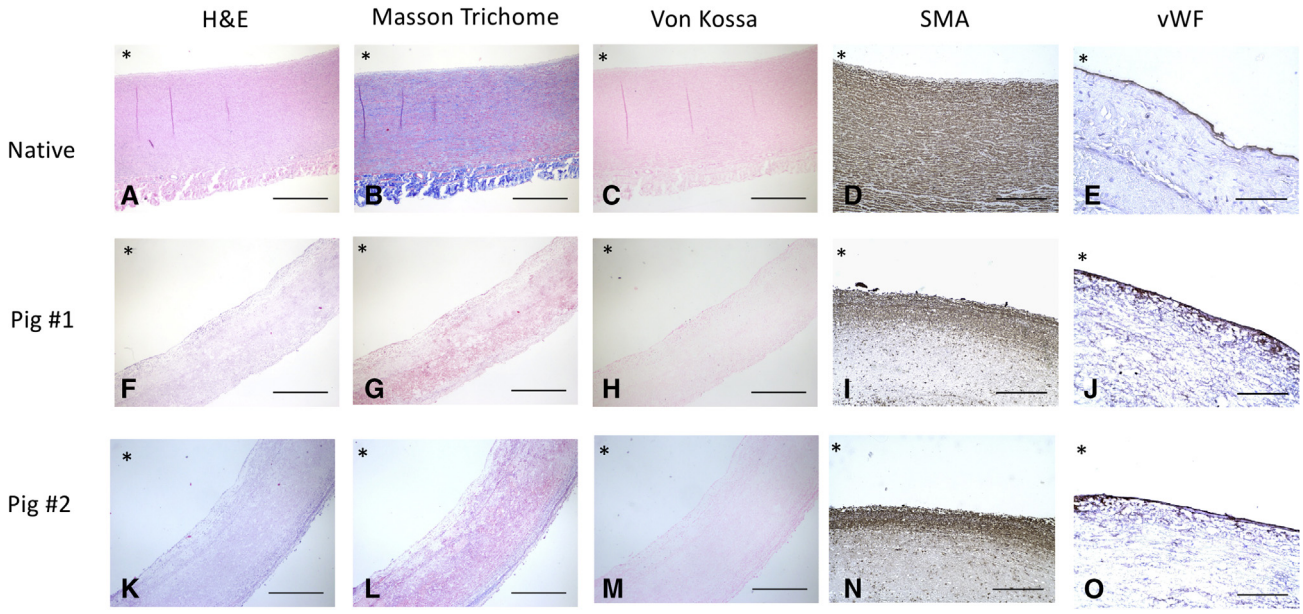

FIGURE 6. Neotissue formation of the vascular graft. A-E, Native pulmonary artery (PA). F-J, Pig 1 graft at the 1-month endpoint. K-O, Pig 2 graft at the 1-month endpoint. *Lumen side. A, F, and K, Hematoxylin and eosin staining of the native PA tissue (A) and the vascular graft (F and K). (Scale bar: 1000 μm.) B, G, and L, Mason trichrome (MT) staining of the native PA (B) and the vascular graft (G and L). (Scale bar: 1000 μm.) The extracellular matrix formation was evaluated with MT staining. Compared with native tissue, the vascular graft showed ongoing extracellular matrix formation. C, H, and M, Von Kossa (VK) staining of native PA (C) and vascular graft (H and M). (Scale bar: 1000 μm.) The staining demonstrated no ectopic calcification. D, I, and N, Smooth muscle actin (*SMA*) staining of the native PA (D) and the vascular graft (I and N). (Scale bar: 500 μm.) The presence of multilayered SMA-positive cells in the graft, which compared with the native pulmonary tissue suggests ongoing active vascular muscle remodeling. E, J, and O, von Willebrand factor (*vWF*) staining of the native PA (E) and the vascular graft (J and O). (Scale bar: 100 μm.) Endothelial cell formation in the graft is shown with the vWF-positive cell in the graft.

macrophages with graft degradation is indicative of the inflammatory process of tissue remodeling in the graft (Figure 7, *A*, center of the graft; *B*, edge of the graft). The percent thickness of the smooth muscle layer (percentage = thickness of smooth muscle/total thickness of the vessel $\times$ 100%) demonstrated some neotissue formation (Figure 7, *C*).

Mechanical Properties of the Customized TEVG Conduit

The mechanical properties of the graft were measured at different time points, including before implantation and 1 month after implantation. The circumferential tensile strength, an analog of the ultimate tensile strength in the tubular structure, of the native tissue and graft after implantation have comparable values: native vs graft (1 month), 0.65 N/mm vs 0.45 N/mm (Figure 7, *D*). The compliance of the graft after implantation was slightly higher than that of the native tissue: compliance, native vs graft (1 month), 9.89% mm Hg vs 21.10% mm Hg (Figure 7, *E*). At the endpoint, the inner diameter of the graft was similar to the inner diameter of the native PA: native vs graft (1 month), 10 mm vs 10 mm (Figure 7, *F*). Due to the short follow-up, the mechanical property measurements of the graft indicate that the customized graft degradation process was in progress with a higher compliance from the remaining scaffold though a similar tensile strength was noted.

DISCUSSION

The results of this study validate the feasibility of the fabrication of the complex-shaped 3D-printed cell-free nanofiber TEVG in an in vivo experiment. We previously demonstrated the capability of creating customized TEVGs using 3D printing and electrospinning technology for straight IVC conduits.[9] Electrospinning provides a unique advantage of using various polymer and fiber sizes to manufacture different-shaped vascular grafts.[12] This study demonstrates that a complex curved and branched "Y" shape conduit can be fabricated by the electrospinning process. In combination with CFD technology, the development of more physiologically compatible patient specific hemodynamics can be achieved.[13]

The materials used in this study showed adequate physical properties in a low-pressure venous system in this in vivo experiment with a 1-month time frame. By optimizing the ratios of the combination of different polymers, the materials can exhibit the advantageous mechanical properties of each individual polymer. The biocompatibility

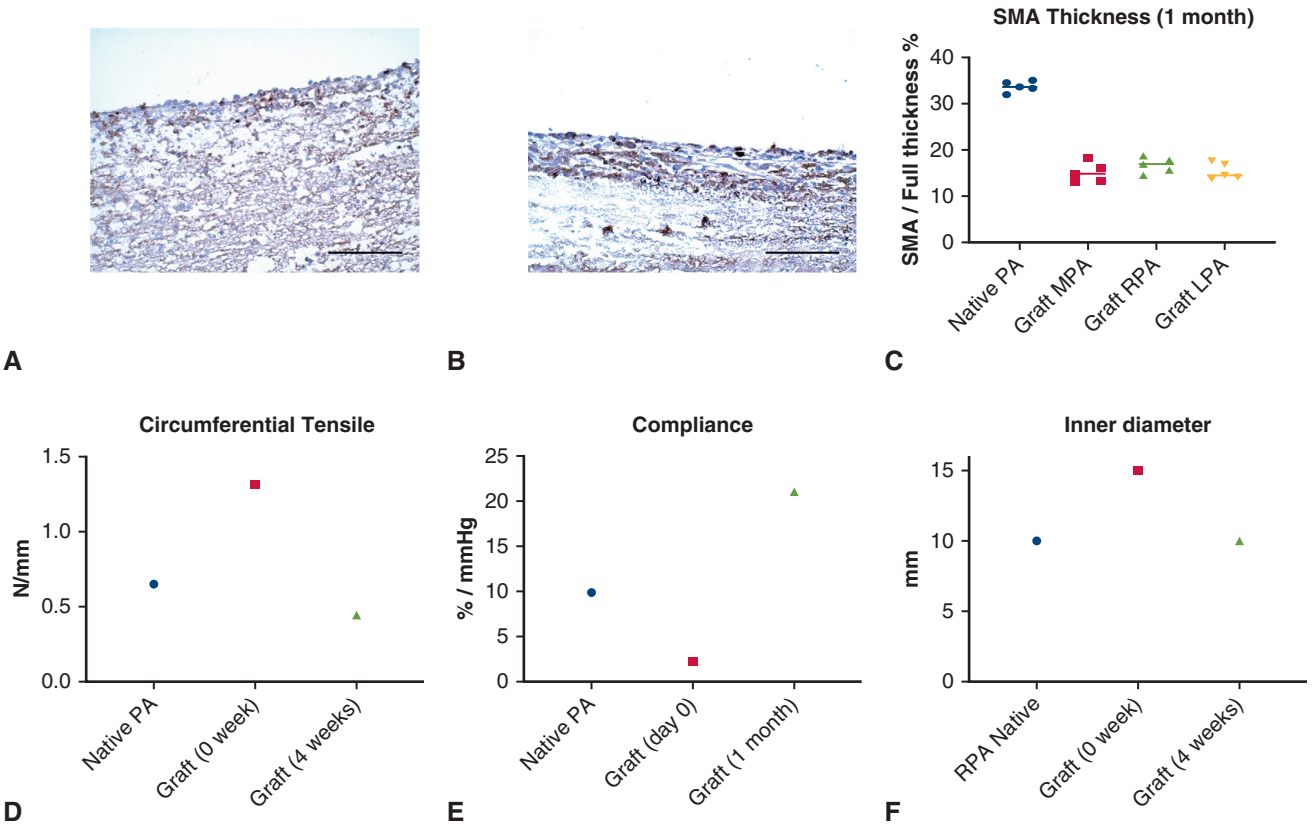

FIGURE 7. Macrophage recruitment inside the graft and mechanical properties of the graft compared with native tissue. A and B, $CD68^{+}$ macrophages seen throughout the graft, including the inside (A) and the edge (B) of the graft. (Scale bar: 100 μm.) The presence of $CD68^{+}$ macrophages with graft degradation is indicative of the inflammatory process of tissue remodeling in the graft. C, The ratio of smooth muscle layer to wall thickness (mean value of native vs MPA vs LPA vs RPA, 33.89 $\pm$ 1.18% vs 15.26 $\pm$ 2.15% vs 16.87 $\pm$ 1.70% vs 15.54 $\pm$ 1.75%). The *middle horizontal line* represents the median; the upper and lower *whiskers*, the maximum and minimum values of nonoutliers. D-F, Mechanical properties of the customized conduit. Native tissue, the PA from the same porcine model; graft (day 0), graft before implantation; graft (1 month), graft at 1 month after implantation. F, Circumferential tensile strength is comparable in the native tissue and graft after implantation: native vs graft (day 0) vs graft (1 month), 0.65 vs 1.31 vs 0.45 N/mm. In B, the compliance of the graft after implantation was slightly higher than that of the native tissue: native vs graft (day 0) vs graft (1 month), 9.89 vs 2.18 vs 21.10% mm Hg. In C, the inner diameter of the graft was comparable to that of the native PA: native vs graft (day 0) vs graft (1 month), 10 vs 15 vs 10 mm. Owing to the limitations of mechanical testing, the tissue samples were destroyed at testing. Only one sample was tested for each parameter. *PA*, Pulmonary artery; *MPA*, main pulmonary artery; *RPA*, right pulmonary artery; *LPA*, left pulmonary artery.

profile of some of the polymers, such as polyglycolic acid (PGA), has been investigated in vivo.[12] Previous human trial used scaffolds with a PGA:PLCL ratio of 1:1.[14] In this study, the materials used to make the TEVG were biodegradable and were previously deployed as scaffolds in the low-pressure circulatory system in patients with congenital heart disease.[15] Because the pressure in the PA is higher than that in the IVC, we used PCL instead of PGA owing to the slower degradation profile, which will allow deposition of more extracellular matrix.[16] We tested the graft with a similar diameter and demonstrated adequate mechanical properties and 1-month survival without graft-related complications. To extend the potential clinical use of this combination of polymers, the in vivo degradation profile of the TEVG made from the combined polymers will be studied in a long-term animal survival study.

One of the innovations of this study is the bifurcated shape of the TEVG. Sugiura and colleagues[17] reported promising results with no graft-related fatal complications in a clinical trial of TEVG use in children with congenital heart disease. That study followed 25 patients who underwent implantation of a linear TEVG as an extracardiac total cavopulmonary conduit for 11 years. The potential benefit would be extended to a larger population of patients who may need curved or even complex-shaped TEVGs. Best and colleagues[18] intended to use a CMR-guided patient-specific TEVG in a 10-year-old patient for total anomalous pulmonary venous return repair,[18] but unfortunately, the excessively complex anatomy made the patient ineligible for linear TEVG clinical use.

This study establishes that the production of a complex-shaped, customized 3D printed and electrospun TEVG is a

feasible technology to manufacture a customized vascular graft with predictable flow dynamics. It would provide the possibility of future development of complex-shaped grafts to fit the anatomy of individual patients.

The goal of TEVG use is to support autologous tissue growth and to remain patent without affecting the blood flow inside the conduit and causing diameter mismatch.[19] Cell-seeded grafts have been investigated to alleviate the intimal hyperplasia in other animal models.[20,21] The dose-related response in cell-seeded grafts also has been advocated for the optimization of cell concentration seeded in the TEVG to prevent the progress of stenosis.[22] In this study, we used a cell-free electrospun nanofiber vascular graft, which demonstrated satisfactory patency and tissue remodeling by 6 months in our previous study of straight TEVG in a sheep model.[9] In this study, we demonstrate complex graft in vivo implantation without stenosis formation over a 1-month period. Our promising data support the need for a study with a longer follow-up period.

The tissue remodeling potential in the graft was demonstrated by the presence of a single layer of endothelial cells, an organized SMC layer, and collagen deposition. As a pilot study, we aimed to demonstrate the feasibility of neotissue formation in a custom-made graft using a porcine model with short term survival of 1 month. Specifically, we found no graft-related mortality and no cases of aneurysm formation, graft rupture, or ectopic calcification using routine imaging modalities for TEVG observation and histological assessment.

In this study, we have proven the feasibility of the in vivo implantation of a complex-shaped, patient-specific TEVG. We have developed several key components, including specific parameters for optimal graft design, unique electrospinning technology, and the technique for surgical experiments using CPB. The novelty of this experiment may provide a potential clinical application in congenital heart surgery, which demands complex-shaped grafts with optimal hemodynamic profiles. Our future work will include a study with a larger number of animals and a longer follow-up period. Our CFD optimization strategy will be refined to evaluate the low-flow regions and areas of low wall shear stress for the susceptibility of thrombosis formation. We will also include different simulation strategies, such as pulsatile flow circulation and hyperdynamic conditions. In the long term, we aim to create an animal model like Fontan physiology that will be amenable to the real clinical encounters, such as vessel stenosis or hypoplasia, to provide a possible application to clinical needs.

In conclusion, we have demonstrated the manufacturability and biocompatibility of the virtual surgical optimization strategy of the 3D-printed patient-specific TEVG conduit in a large animal model. Although this study was limited by its short survival duration and small sample number, the results are promising and definitely warrant further investigation.

Webcast

You can watch a Webcast of this AATS meeting presentation by going to: https://aats.blob.core.windows.net/media/19%20AM/Monday_May6/202BD/202BD/S85%20-%20Expandable%20prostheses%20for%20growing/S85_4_webcast_030446662.mp4.

Conflict of Interest Statement

J. Opfermann, J. Johnson, A. Krieger, and N. Hibino are inventors listed on International Patent WO/2017/035500Al (Patient-Specific Tissue Engineered Vascular Graft Utilizing Electrospinning). The patent filing has been disclosed for grant applications and to institutions. J. Johnson and N. Hibino are equity holders in Nanofiber Solutions. All other authors have nothing to disclose with regard to commercial support.

We thank Dr Henry Halperin, Dr Cecillia Lui, Dr Sara Abdollahi, Tom Loke, Melissa Jones, and Sean Kearney for their surgical support and Dr Ehud Schmidt, Michael Guttman, Rick Tunin, and Sarah Fink for perioperative surgical support and veterinary imaging technical expertise. We also acknowledge the University of Maryland supercomputing resources (http://hpcc.umd.edu/) that were made available for conducting the research reported in this article.

References

1. Benjamin EJ, Blaha MJ, Chiuve SE, Cushman M, Das SR, Deo R, et al. Heart disease and stroke statistics—2017 update: a report from the American Heart Association. *Circulation*. 2017;135:e146-603.
2. Dearani JA, Danielson GK, Puga FJ, Schaff HV, Warnes CW, Driscoll DJ, et al. Late follow-up of 1095 patients undergoing operation for complex congenital heart disease utilizing pulmonary ventricle to pulmonary artery conduits. *Ann Thorac Surg*. 2003;75:399-410; discussion 410-1.
3. Karamlou T, Blackstone EH, Hawkins JA, Jacobs ML, Kanter KR, Brown JW, et al. Can pulmonary conduit dysfunction and failure be reduced in infants and children less than age 2 years at initial implantation? *J Thorac Cardiovasc Surg*. 2006;132:829-38.
4. Poynter JA, Eghtesady P, McCrindle BW, Walters HL III, Kirshbom PM, Blackstone EH, et al. Association of pulmonary conduit type and size with durability in infants and young children. *Ann Thorac Surg*. 2013;96:1695-701; discussion 1701-2.
5. Caldarone CA, McCrindle BW, Van Arsdell GS, Coles JG, Webb G, Freedom RM, et al. Independent factors associated with longevity of prosthetic pulmonary valves and valved conduits. *J Thorac Cardiovasc Surg*. 2000;120:1022-30; discussion 1031.
6. Ovroutski S, Ewert P, Alexi-Meskishvili V, Stiller B, Nürnberg JH, Abdul-Khaliq H, et al. Comparison of somatic development and status of conduit after extracardiac Fontan operation in young and older children. *Eur J Cardiothorac Surg*. 2004;26:1073-9.
7. Downing TE, Allen KY, Goldberg DJ, Rogers LS, Ravishankar C, Rychik J, et al. Surgical and catheter-based reinterventions are common in long-term survivors of the Fontan operation. *Circ Cardiovasc Interv*. 2017;10:e004924.

8. Petrossian E, Reddy VM, McElhinney DB, Akkersdijk GP, Moore P, Parry AJ, et al. Early results of the extracardiac conduit Fontan operation. *J Thorac Cardiovasc Surg*. 1999;117:688-96.
9. Fukunishi T, Best CA, Sugiura T, Opfermann J, Ong CS, Shinoka T, et al. Preclinical study of patient-specific cell-free nanofiber tissue-engineered vascular grafts using 3-dimensional printing in a sheep model. *J Thorac Cardiovasc Surg*. 2017;153:924-32.
10. Siallagan D, Loke YH, Olivieri L, Opfermann J, Ong CS, de Zélicourt D, et al. Virtual surgical planning, flow simulation, and 3-dimensional electrospinning of patient-specific grafts to optimize Fontan hemodynamics. *J Thorac Cardiovasc Surg*. 2018;155:1734-42.
11. Alsoufi B. Right ventricle-to-pulmonary artery conduits: do we really have an option? *J Thorac Cardiovasc Surg*. 2016;151:442-3.
12. Rocco KA, Maxfield MW, Best CA, Dean EW, Breuer CK. In vivo applications of electrospun tissue-engineered vascular grafts: a review. *Tissue Eng Part B Rev*. 2014;20:628-40.
13. de Zélicourt DA, Marsden A, Fogel MA, Yoganathan AP. Imaging and patient-specific simulations for the Fontan surgery: current methodologies and clinical applications. *Prog Pediatr Cardiol*. 2010;30:31-44.
14. Hibino N, McGillicuddy E, Matsumura G, Ichihara Y, Naito Y, Breuer C, et al. Late-term results of tissue-engineered vascular grafts in humans. *J Thorac Cardiovasc Surg*. 2010;139:431-6. 436.e1-2.
15. Freed LE, Vunjak-Novakovic G, Biron RJ, Eagles DB, Lesnoy DC, Barlow SK, et al. Biodegradable polymer scaffolds for tissue engineering. *Biotechnology (N Y)*. 1994;12:689-93.
16. Van de Velde K, Kiekens P. Biopolymers: overview of several properties and consequences on their applications. *Polym Test*. 2002;21:433-42.
17. Sugiura T, Matsumura G, Miyamoto S, Miyachi H, Breuer CK, Shinoka T. Tissue-engineered vascular grafts in children with congenital heart disease: intermediate term follow-up. *Semin Thorac Cardiovasc Surg*. 2018;30:175-9.
18. Best C, Strouse R, Hor K, Pepper V, Tipton A, Kelly J, et al. Toward a patient-specific tissue engineered vascular graft. *J Tissue Eng*. 2018;9. 2041731418764709.
19. Fukunishi T, Best CA, Ong CS, Groehl T, Reinhardt J, Yi T, et al. Role of bone marrow mononuclear cell seeding for nanofiber vascular grafts. *Tissue Eng Part A*. 2018;24:135-44.
20. Mirensky TL, Hibino N, Sawh-Martinez RF, Yi T, Villalona G, Shinoka T, et al. Tissue-engineered vascular grafts: does cell seeding matter? *J Pediatr Surg*. 2010;45:1299-305.
21. Roh JD, Sawh-Martinez R, Brennan MP, Jay SM, Devine L, Rao DA, et al. Tissue-engineered vascular grafts transform into mature blood vessels via an inflammation-mediated process of vascular remodeling. *Proc Natl Acad Sci U S A*. 2010;107:4669-74.
22. Lee YU, Mahler N, Best CA, Tara S, Sugiura T, Lee AY, et al. Rational design of an improved tissue-engineered vascular graft: determining the optimal cell dose and incubation time. *Regen Med*. 2016;11:159-67.

Key Words: 3D printing graft, customized branched TEVG, CFD optimization, neotissue formation, in vivo implantation of TEVG

Discussion

Dr Glen Van Arsdell *(Los Angeles, Calif)*. Dr Yeung, I rise to congratulate you and your coauthors on your innovative work. I literally have no criticism. This is exactly what we should be doing as a Society, taking technology that's ready to be tested and trying to find a use for it. Obviously when you start something, there are problems to work out, and so really my questions are around how do you see this moving forward to deal with some of the issues that you saw.

Your initial work was on an IVC venous system and then you have moved to a moderate pressure system with a demonstrated lower collagen content. Do you suppose there are some tissue engineering methods by which you can make this applicable to a systemic side, is that conceivable, and how would you go about that?

Dr Enoch Yeung *(Baltimore, MD)*. Thank you for your question. Actually, in our previous study of the implantation in a sheep model, the graft was made from PGA and PLCL, but in this experiment the graft was made from PSCL and also PLCL. We used PCL instead of PGA because PCL has a slower degradation profile, which can stay longer in the graft, and we hope that it can provide a better mechanical property to the graft in this study. And we used the same materials, PGA and PLCL, to create a graft in a high-pressure system in another large model animal. This paper is now in the review process.

Dr Van Arsdell. When you look at the pictures, I know there is demonstration of neointima or endothelial formation, but it actually looks a little bit different. Do you have any thoughts about that and what you might be doing in the future to solve that issue?

Dr Yeung. Thank you for your question and suggestion. We agree that actually the new tissue formation in the graft is not exactly as what we expected in the tissue remodeling. We believe that there was an ongoing tissue remodeling process in this experiment. We are now working on the same animal model with longer survival and longer follow-up. We are eager to see and also want to evaluate how the tissue remodeling in this neointima will be in long-term follow-up.

Dr Van Arsdell. Thank you for innovative work and comments.

Dr Yeung. Thank you.

Dr John E. Mayer *(Boston, Mass)*. I agree. I think this is really exciting. This is bringing several technologies together to be able to custom make a graft for a given patient.

I have a few technical questions. One is how big are the fibers that you are printing, what is the fiber diameter?

Dr Yeung. You are talking about nano fiber diameter, right?

Dr Mayer. Very small. How many microns?

Dr Yeung. I'm sorry, I don't remember the exact number, but I would like to come back to you with the exact number.

Dr Mayer. The reason that I ask, and I think it is illustrative of a more general principle, is that we know that the cells are going to react quite differently depending on

what the diameter of the fiber is that they attach to, and since most cells are in the 10 to 20 micron size dimension, anything much bigger than that is going to be perceived as a flat surface rather than a fiber, which affects how the cells behave. This is one of the innumerable challenges in trying to design these kinds of grafts.

As Toshi so kindly pointed out, we have been working in this field for over 20 years, and the only thing I can say with any degree of definitiveness is that the more you know the more you don't know. I think that's the real challenge for trying to devise a graft that can work in a very complicated biological environment. There is enough to keep another generation of investigators going, I would say, for sure.

I do think another important question is whether or not we start decorating these fibers with chemical complexes so that you can then start guiding the cellular behavior more completely. Thank you.

Dr Yeung. Thank you for your comment.

Unidentified Speaker. One very quick question, just technical. Is the printer you use commercially available, or is it designed to print the particular polymers that you are using?

Dr Yeung. Actually, in this experiment, all we used is PCL and PLCL, but with the same printer we can do another printing, use the same initial printing, or with another nano polymer.

Unidentified Speaker. So is this a commercially available printer or is it a custom-made printer for your project?

Dr Yeung. It is a kind of custom-made 3D printer, because as you can see, our graft is branched. We have to adjust how we can do the electrospinning. It is not common that the commercial 3D printer can do the branched 3D printing.

APPENDIX E1. CALCULATION METHOD FOR REMAINING SCAFFOLD

The remaining scaffold percentage was calculated as follows. The remaining scaffold was measured as light intensity under standardized condition including same light exposure and the exposure time. The intensity measured was converted into pixel count by ImageJ, with the exclusion of background noise in each individual slide owing to the intrinsic impurity of the slides. The maximal pixel count determined by ImageJ was set to be the original undegraded graft pixel. The percentage was calculated as pixel of graft/pixel of the undegraded graft × 100%.

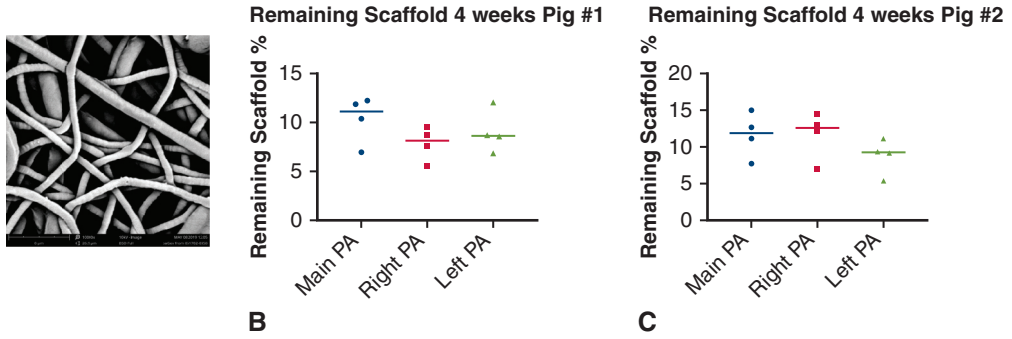

FIGURE E1. A, Nanofiber of the graft with reference size. (Scale bar: 8 μm). B and C, The remaining scaffold percentage in individual part of the graft of pig 1 and pig 2 were measured. The average of the remaining scaffold of main pulmonary artery (PA; *blue*), right PA (*red*), and left PA (*green*) were 11.0 ± 2.64, 9.76 ± 3.18, and 8.93 ± 2.14, respectively, in pig 1 and 11.0 ± 2.64, 9.76 ± 3.18, and 8.93 ± 2.14, respectively, in pig 2.